Analysis of Atmospheric Aerosols Collected in an Urban Area in Upstate NY Using Proton Induced X-ray Emission (PIXE) Spectroscopy

By

Jeremy Wayne Smith

****

Submitted in Partial Fulfillment

of the requirements for

Honors in the Department of Physics and Astronomy

UNION COLLEGE

June, 2014

ABSTRACT

SMITH, JEREMY Analysis of Atmospheric Aerosols Collected in an Urban Area in Upstate NY Using Proton Induced X-ray Emission (PIXE) Spectroscopy

ADVISOR: LABRAKE, SCOTT

We have performed a PIXE analysis of atmospheric aerosol samples collected in Schenectady, NY, to study airborne pollution in an urban environment. The samples were collected using a PIXE International, 9-stage, cascade impactor that separates the airborne particles according to aerodynamic diameter and deposits them on thin Kapton foils. The impacted foils were bombarded with 2.2-MeV proton beams from the Union College 1.1-MV Pelletron accelerator and the emitted X-rays were detected with an Amptek silicon drift detector. The X-ray energy spectra were analyzed using GUPIX software to determine the elemental concentrations in the samples. A broad range of elements from Al to Pb were identified and measurable concentrations of Br and Pb were detected at small particle sizes. The measured Br/Pb ratio of 0.37±0.04 is consistent with results from previous studies and suggests the presence of leaded aviation fuel that may be due to the proximity of the collection site to a small regional airport with a significant amount of general aviation traffic.

1 Introduction

1.1 Motivation

In the past couple of decades it has become increasingly important to preserve our planet and be self-aware of the waste we produce and the harm that we are doing to the environment. One of the biggest steps taken in an attempt to help keep our planet clean was the U.S. Clean Air Act initiated in 1967. This act was designed to control the air pollution from products that are harmful to our atmosphere. One of the things it did was to ban the sale of leaded fuel for use in on-road vehicles. Leaded fuel is regular motor fuel that has tetraethyl lead as an additive in order to prevent damage to the engine from "engine knocking." Knocking is when the gasoline in the engine produces uncontrolled combustion which cannot be used to power the engine and can often damage the engine. Lead was first added to gas in the 1920s because it prevented knocking without reducing the efficiency of the gasoline. When the extent of the environmental and health damage caused by the lead emission was realized, leaded gasoline was phased out for automobiles in 1973. However, automobiles were not the only vehicles that used leaded fuel. Small general aviation aircraft use spark-ignited internal-combustion engines which are similar to engines used by automobiles; whereas larger passenger jet aircraft use engines that do not use spark-ignition and therefore do not need the lead in the fuel to prevent knocking. Therefore smaller aircraft tend to use aviation gasoline which contains tetraethyl lead in order to prevent the knocking of the engine. In this paper we will be examining aerosol samples collected from Schenectady NY in order to see if the leaded gasoline used by small aircrafts from the local airport is affecting our environment.

Specifically, the airport we will be looking at is the Schenectady County Airport because it uses 100LL Jet-A fuel. The LL stands for low lead and this fuel is used for the smaller aircrafts. Schenectady County Airport has around 136 small aircraft take off and landings each day so we expect to see lead in the air due the emission from these small aircraft[11]. We will be looking for four results throughout this experiment: if we can detect any Pb in the air samples by particle induced x-ray emission spectroscopy, if Pb is detected, can we identify it as being from tetraethyl lead used in aviation gas, and

whether or not the Pb concentrations vary by season or by the location with respect to the airport. There have been previous studies primarily in the 70's on looking for lead in the air in other areas of the world. One such paper was examining the lead pollution due to leaded fuel in gas in Australia.[1-2] O'Conner et al also compared the elemental concentration contaminated by car emission to pollution due to factories and other forms of pollution. O'Connor et al found that the emission from cars using leaded gas was unique in that it had both Pb and Br. They also looked at emission from industry and observed that there was only Pb in the air and no Br. There is Br in the leaded fuel from lead(ll) bromide which is an additive used to prevent the resulting Pb oxides from fouling the engine. O'Connor et al found there to be different ratios of Br/Pb corresponding to how much of leaded fuel emissions there were. In Perth Australia during the 1970s, there was still leaded fuel being used in automobiles which corresponded to a mean Br/Pb ratio of 0.59±0.05; while in the US during the 70s, there was only leaded fuel being used in small aircrafts and the average measured Br/Pb ratio was 0.25±0.03. If we see a ratio in between the ratios from Australia and the US we will be able to identify it as leaded fuel emission.

1.2 Proton Induced X-Ray Emission Spectroscopy

Proton Induced X-ray Emission Spectroscopy or PIXE is a non-destructive elemental analysis technique. PIXE is a standard nuclear physics technique for determining elemental makeup of an unknown target with elements ranging from Al to U. We chose to use this method because we can preserve and rerun our samples and it is a very effective method for examining very small samples since we can shape and steer the beam very accurately. PIXE involves the process of a proton interacting with an electron in a target atom causing an electron to be ejected from its electron shell. When an electron is removed from its orbital then there is a vacancy that will be filled by another electron from a higher electron orbit. To do this an electron from a higher order shell will de-excite to fill the vacancy, and this transition which conserves energy, produces an x-ray equal to the difference in the energies of the electron shells, and is shown in Figure 1. This difference in energies is unique for every element due to the fact that every element will have a different number of protons in its nucleus and will therefore induce a different

coulomb force on the electrons. We can therefore determine what element emitted the X-ray due to the interaction with the proton.

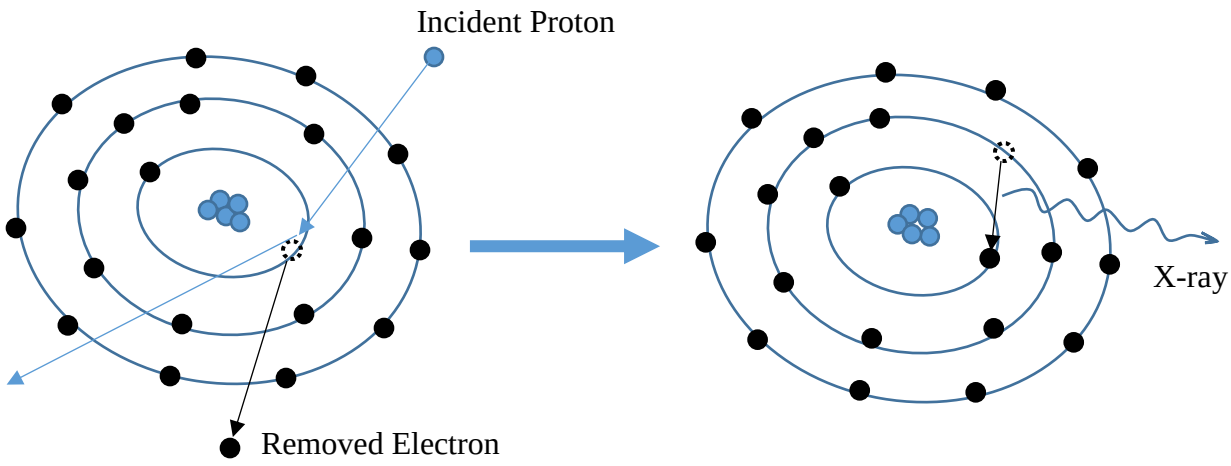

Figure 1: Cartoon diagram showing an incident proton interacting with an electron of the inner most shell and then an electron from a higher order electron shell emitting an X-ray in order to fill the vacancy left from the emitted electron.[3]

There are different transitions in each atom, based on probabilities, which can occur depending on what shell the electron is ejected from and where the "replacement" electron originates. The transitions can be split up into series which correspond to the electron shell that the electron was ejected: K if it was the inner most shell or the n=1 state, L if it was the second shell or the n=2 state, M if it was the third shell or the n=3 state and so on as shown in Figure 2, where the shells are based on the Bohr model of the atom. K transitions are the most common in lighter elements; however, once you get to the heavier elements, such as Sn and Au, it is harder to knock an electron out of the inner shell because the nucleus is larger and therefore there is a greater attractive force holding the electrons in orbit which would require a higher proton beam energy to remove. Therefore it is more common to see L transitions in heavier elements which are transitions into the n=2 state. Further transitions can also be categorized by which orbital the electron transitions from in order to fill the vacancy left by the ejected electron. The most common transition is also the lowest energy transition and the one that has the highest probability, and is called an α transition. The electron can also transition from higher electron shells; if it is two energy levels away it is termed a β transition, if it is three shells away it is a γ transition and so on as shown in Figure 2.

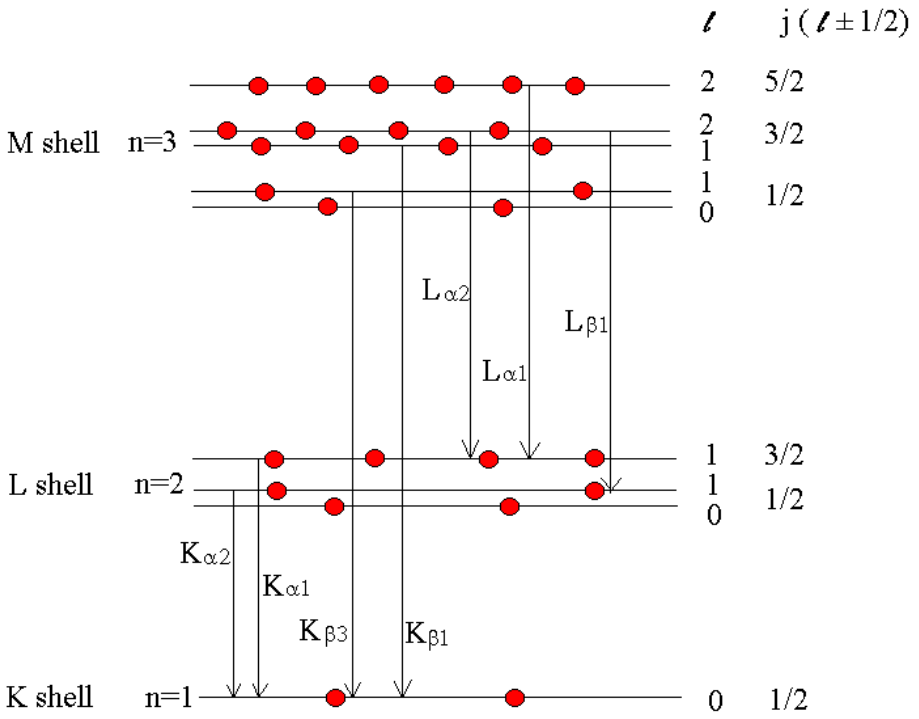

Figure 2: The electron transitions that can occur during PIXE. The letters corresponds to the shell that the electron was ejected from due to the incident proton while the Greek letter designations corresponds to the shell that the electron which filled the vacancy originates and the number corresponds to the spin of the electron that filled the vacancy.[4]

The energy of the emitted X-ray from the electron transition is defined as

$$\Delta E_{x-ray} = E_{upper\ state} - E_{lower\ state} \qquad [1]$$

where the upper and lower states refer to the higher and lower energy states of the transition electron respectively. As a first order treatment we apply the Bohr theory to determine the total energy of a state, which is the sum of the kinetic and potential energies in terms of the quantized orbits. The total energy is therefore,

$$E_n = KE + PE = \frac{1}{2}m\left(\frac{Ze^2}{4\pi\varepsilon_0 n\hbar}\right)^2 - \frac{Ze^2}{4\pi\varepsilon_0\left[\frac{4\pi\varepsilon_0 n^2\hbar^2}{mZe^2}\right]} = -\frac{Z^2me^4}{2(4\pi\varepsilon_0)^2n^2\hbar^2} \qquad [2]$$

where m is the mass of an electron, e is the charge of an electron, Z atomic number of the target atom, and n is the principle quantum number designating the electron orbit. The

term in parenthesis is the quantized expression for the velocity of the electron in orbit and the term brackets is the quantized radius. This equation describes the dynamics of a K transitions, for a hydrogen-like atom. However, in an actual atom containing many electrons, we take into account that the transitioning electron is shielded from the nucleus by the remaining n=1 state electron. We can account for this by substituting a Z-1 for the Z variable to represent both the protons in the nucleus acting on the electron and the remaining electron in the orbital. We can then substitute values for all our known values, such as *m*, *e*, etc, to get

$$E_n = -\left(\frac{me^4}{2(4\pi\varepsilon_0)^2\hbar^2}\right)\frac{(Z-1)^2}{n^2} = -13.57eV\left(\frac{(Z-1)^2}{n^2}\right) \quad [3]$$

By combining equations 1 and 3 and evaluating all of the constants we get the energy of the emitted X-ray to be the following

$$\Delta E_{x-ray} = -13.57eV \cdot (Z-1)^2\left[\frac{1}{n_{lower}^2} - \frac{1}{n_{upper}^2}\right] \quad [4]$$

This equation can be used to calculate the energies of the X-rays emitted for all K-transitions. Using equation 4, one can find the x-ray energy of a K-transition for a specific element. There is a similar calculation that can be done for L, M, and other various transitions such as α and β but it is a lot more complicated and requires the use of quantum physics. Energies for all electron transitions have been previously calculated and from calibrated x-ray energy spectra we can look up the elemental identity corresponding to a known energy transition, based in part on equation 4.

We will also want to be able to measure the concentrations of the elements we find so that we know how much of each element was actually in our sample. We will use the following equation in order to measure the concentration, C_z, in units of ng/cm^2.

$$C_Z = \frac{Y_Z}{Y_T \cdot H \cdot Q \cdot \varepsilon \cdot T} \quad [5]$$

where C_Z is the concentration of each of the elements *Z*, Y_Z is the intensity of the principle X-ray line, Y_T is the theoretical intensity based on the width of the peak, *H* is an experimental constant equal to the solid angle of the detector, *Q* is the total charge

collected, ε is the efficiency of the x-ray detector and T is the transmission coefficient through any filters or absorbers between the sample and the X-ray detector.[5]

2 Procedure

2.1 Collection and Preparation of Samples

We collected aerosol samples from two different sampling sites near Schenectady airport as a function of time of the year. We did this to see if we could detect Pb in the air samples and if we could identify any Pb found as being from tetraethal lead and if the concentration of Pb varied by season or by location with respect to the airport. We collected a total of 7 sets of samples from the Union College Boathouse (sample site 1) which is about 2 miles south of the main runway at the Schenectady County Aiport and 1 set of samples from a local residence about 0.5 miles east of the main runway (sample site 2) as shown in Figure 3. Most aircraft traffic flows along the compass heading of 220° (SSW) having them land on the heading SSW and take off on heading SSW, generally turning right away from Albany. We took data from sampling site 2 because we wanted to see if there was any lead detected perpendicular to the main runway. In order to collect our aerosol samples we used a PIXE international nine-stage cascade impactor as shown in Figure 4. The impactor works by pulling air through 9 stages and the stages collect specific particles based on their aerodynamic size. We can collect a range of particle sizes from 0.06μm (stage L1) to 16μm (stage 7). The collected particles from each stage are deposited onto 7.5μm thick Kapton foils as shown in Figure 5. The Kapton foils are examined using PIXE in order to determine concentrations (in ng/cm^2) of the elements present. However, in order to get an accurate picture of how much of each element is present in a volume of air we breathe we need to determine the concentrations of each element in ng/m^3. To do this, we used information gathered on the days that we took the samples, such as temperature, pressure, and flow rate, and the following equation

$$Conc_{volume} = \left(\frac{P_{STD}}{T_{STD} \cdot time}\right)\left(\frac{Conc_{area} \cdot A \cdot T}{P \cdot flow}\right) \qquad [6]$$

where P_{STD} and T_{STD} are standard pressure and temperature equal to 760mmHg and 298K respectively, $Conc_{area}$ is the concentration per unit area in terms of ng/cm^2, time is the amount of time the impactor was collecting particles in minutes, A is the area of the deposit left on the Kapton foil as shown in Figure 5, T and P are the average temperature and pressure while the impactor was collecting particles and flow is the flow rate of the air through the impactor which was equal to 1L/min or 0.001m^3/min.

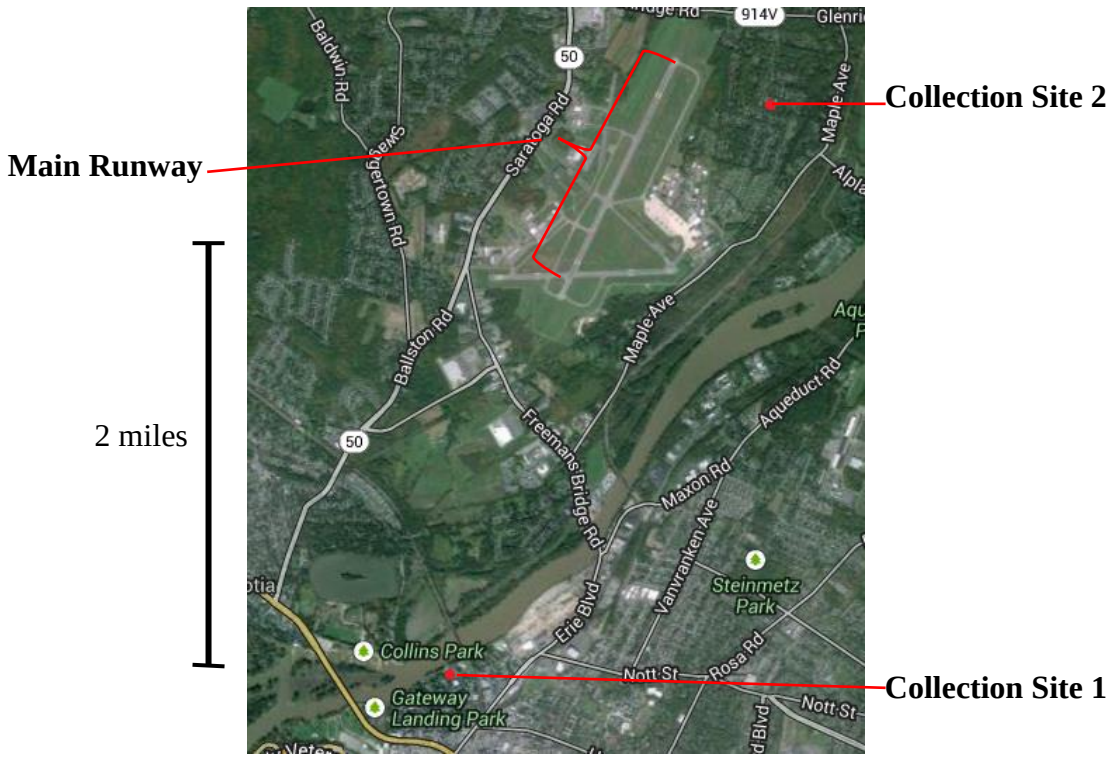

Figure 13: Picture of the main runway of the Schenectady County Airport showing collection site 1, the Union College Boat House parallel to the main runway, and collection site 2, perpendicular to the runway.[6]

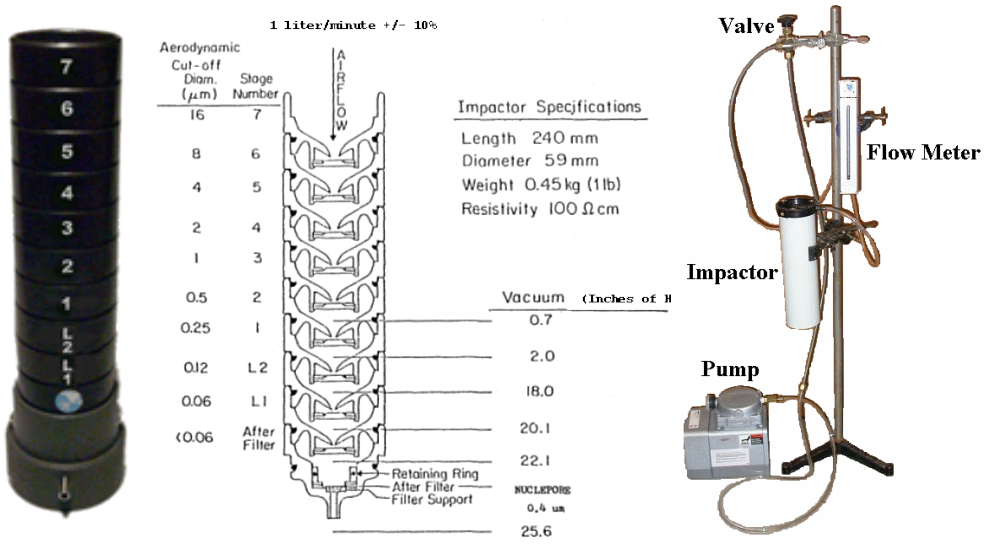

Figure 4: On the far left, is a picture of the nine stage cascade impactor which works by drawing air from the top, at stage 7, and pulls the air through the 9 stages. The middle schematic shows a cross-section of the impactor along with each stages' aerodynamic particle cutoff size. The picture on the far right shows the impactor fully set up with a pump pulling air through the impactor from the bottom towards the top.[7]

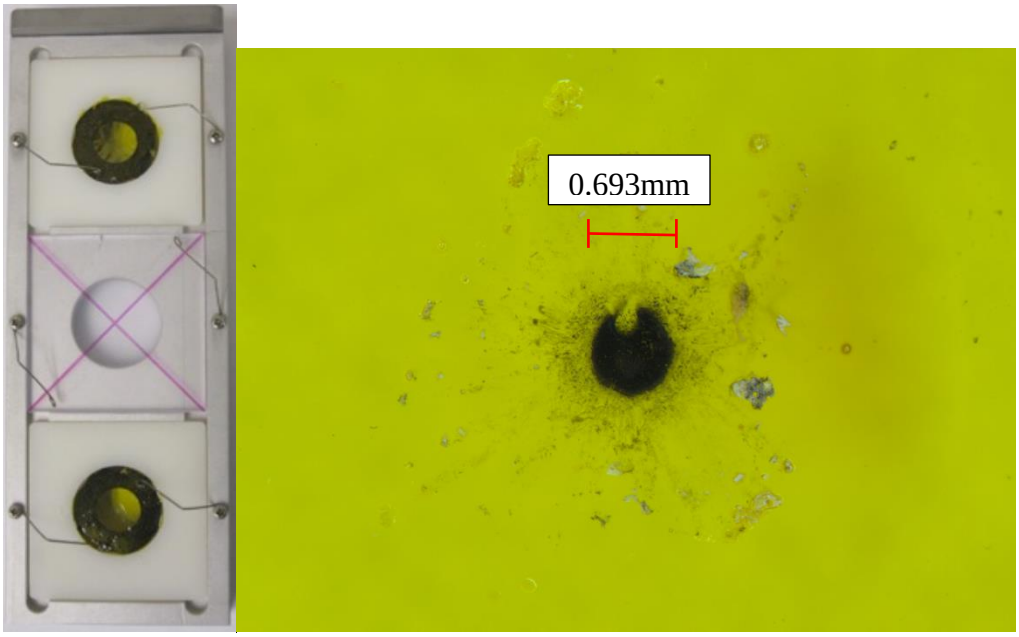

Figure 5: On the left is a picture of the target ladder holding two Kapton foils on the top and bottom and a plastic scintillator target in the center for centering the beam. On the right is a magnified picture of an aerosol deposit spot on one of the Kapton foils.

2.2 Particle Accelerator

For this experiment we will be using a NEC 1.1MV tandem electrostatic particle accelerator, shown in Figure 6. This particle accelerator has the ability to accelerate protons to energies of 2.2MeV. For our experiment we will be using protons, so we will start with hydrogen gas which is fed into a quartz bottle. A radio frequency discharge of 100mHz is supplied to the hydrogen gas in the quartz bottle to produce a plasma of positive ions. This occurs by stripping the electrons from the proton in the hydrogen gas. A voltage difference, in the range of 2-6 kV, accelerates the protons from the quartz bottle into the Rb furnace as shown in Figure 7. In the Rb furnace, a low density vapor of Rb is produced. The atoms of this Rb vapor have very loosely bound valence electrons. Through charge-exchange collisions, the protons gain two extra electrons producing H^- before being injected into the main section of the accelerator shown in Figure 8.

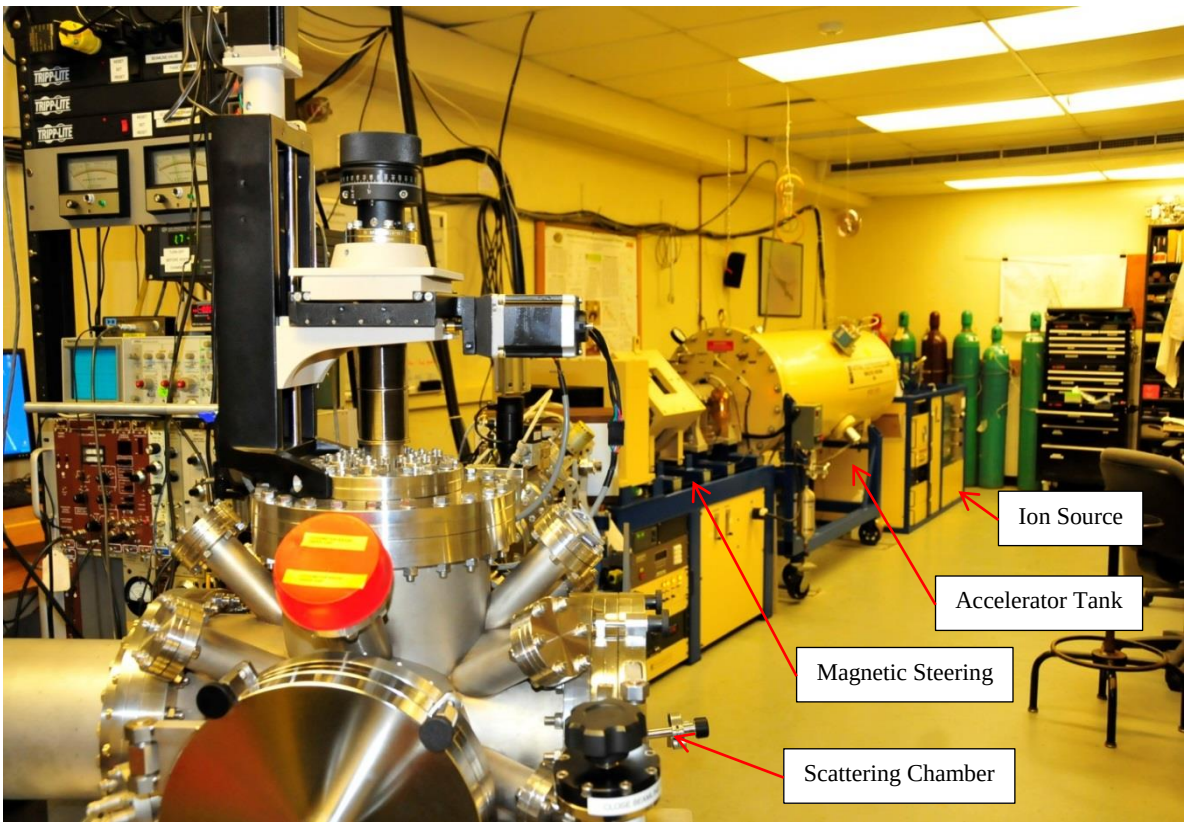

Figure 6: A picture of the Union College 1.1MV tandem Pelletron particle accelerator. The particles begin on the right side of the figure in the ion source and then are accelerated through the tank and magnetically steered until they reach the scattering chamber at left end.

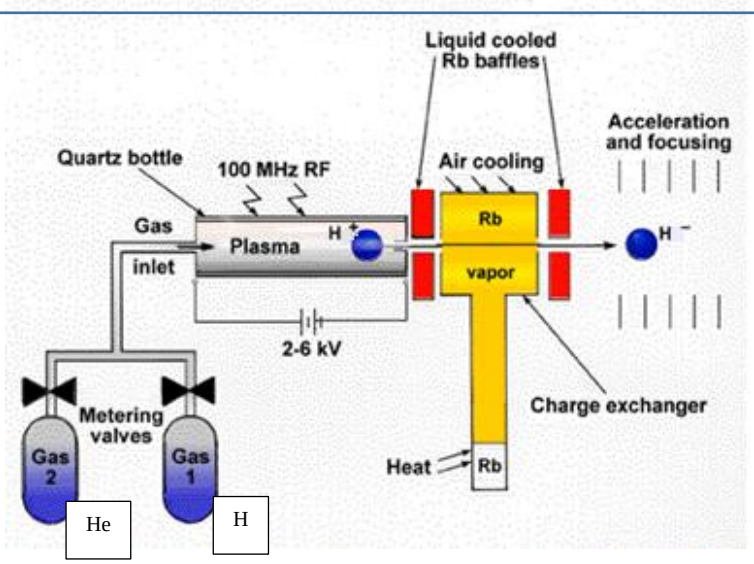

Figure 7: Schematic of the ion source Hydrogen gas being fed into the quartz bottle across which 2-6kV potential difference can be applied. This extracts the H^+ into the Rb furnace where the ions pick up two electrons through charge exchange collisions becoming H^- and injects them into the accelerator.[8]

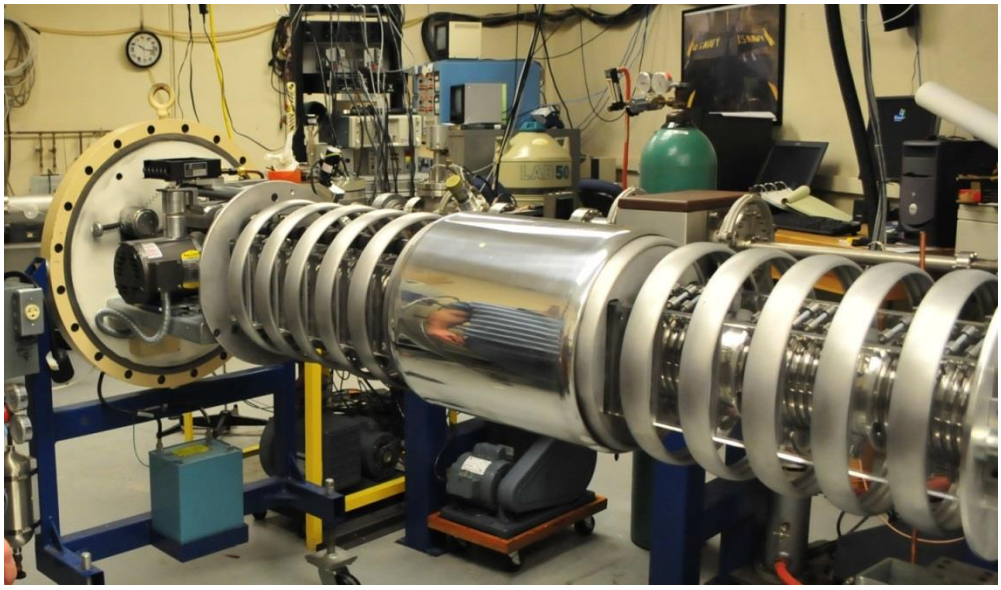

Figure 8: A picture of the inside of the accelerator tank showing the terminal shell in the middle which has a static positive charge and causes the negatively charged protons to be accelerated towards it with 1.1MeV of work being done on the protons. Then, low density nitrogen gas is bled to the terminal which strips the electrons and the protons are then accelerated away from the terminal with another 1.1MeV of work being done on the protons.

The accelerator itself is a tandem electrostatic machine with a positive terminal potential of up to 1.1MV. The Pelletron charging system charges the terminal by induction and the chain inside of the pressure tank consists of metal pellets connected together by insulating links. The negatively charged inductor electrode pushes electrons off the pellets while they are in contact with the grounded drive pulley. Since the pellets are still inside the inductor field as they leave the pulley they retain a net positive charge. The chain then transports this charge to the high-voltage terminal where the reverse process occurs. When it reaches the terminal, the chain passes through a negatively biased suppressor electrode that prevents arcing as the pellets make contact with the terminal pulley. As the pellets leave the suppressor, charge flows smoothly onto the terminal pulley giving the terminal a net positive charge. When the protons with their extra negative charges enter from one side they are accelerated through the first half of the accelerator which has a 1.1 MV potential difference and 1.1 MeV of work is done on the proton by the terminal. At the terminal a low density nitrogen gas is bled in from an outside source and this strips the protons of their two electrons, again through charge exchange collisions. The protons are then accelerated through the second half of the accelerator and this results in another 1.1MeV of work on the proton. We can then calculate the total work being done on the particle using the following equation

$$W_{total} = [1e^{+} \times (3.6kV)] + [(-1e^{-}) \times (-1.1MV)] + [1e^{+} \times (1.1MV)] = 2.2MeV \quad [7]$$

where the first term is the work done across the source, the second term is the work done across the low energy portion of the accelerator and the third term is the work done across the high energy portion of the accelerator. We can then use this to find how fast the protons are moving using the following equations

$$W_{total} = KE_f - KE_i = 2.2MeV \times \frac{1.6\times10^{-19}J}{1eV} = 3.52 \times 10^{-13}J = (\gamma - 1)m_p c^2 \quad [8]$$

We then solve this equation to get a value of 1.0023 for γ and we can then solve for the velocity of the proton using the following equation

$$v_p = \sqrt{\frac{\gamma^2-1}{\gamma^2}} = 0.0683c = 2.048 \times 10^7 m/s \quad [9]$$

Note that we did not need to take into account relativistic effects since the protons are traveling fast at a speed less than 0.1c. Our beam of protons now has an energy of 2.2MeV and a speed of 2.048×10^{7} m/s as it enters the steering magnets and scattering chamber.

After the proton beam leaves the accelerator it then passes through two sets of quadrapole magnets which are used to shape the beam as shown in Figure 9. We made the beam circular since the deposit spots were roughly circular. While our accelerator should have accelerated all our protons to have energy of 2.2MeV, there may still be other particles, such as N, O, or Rb, or protons of different energies due to the spread in the energy of the beam. We filter the particle beam to get the protons that have energy of 2.2MeV by magnetically steering the protons we want into the scattering chamber. Finally the beam enters the scattering chamber where the samples are placed in a three sample target ladder and the Amptek X-ray detector is located 135 degrees from the incident direction as shown in Figure 10. The samples are placed on a target ladder connected to a mechanical arm that can move the slide in a place perpendicular to the beam, parallel to the beam and can be rotated through the beam. The ladder holds up to three samples at a time so we can take data on one sample and then move the mechanical arm so that we can take data on the next sample. Once the proton beam hits the sample the X-rays are emitted through the PIXE process and are then detected by the Amptek X-ray detector in the scattering chamber. There is a 76μm Be window in front of the detector in order to remove the low energy x-rays and scattered charged particles (protons).

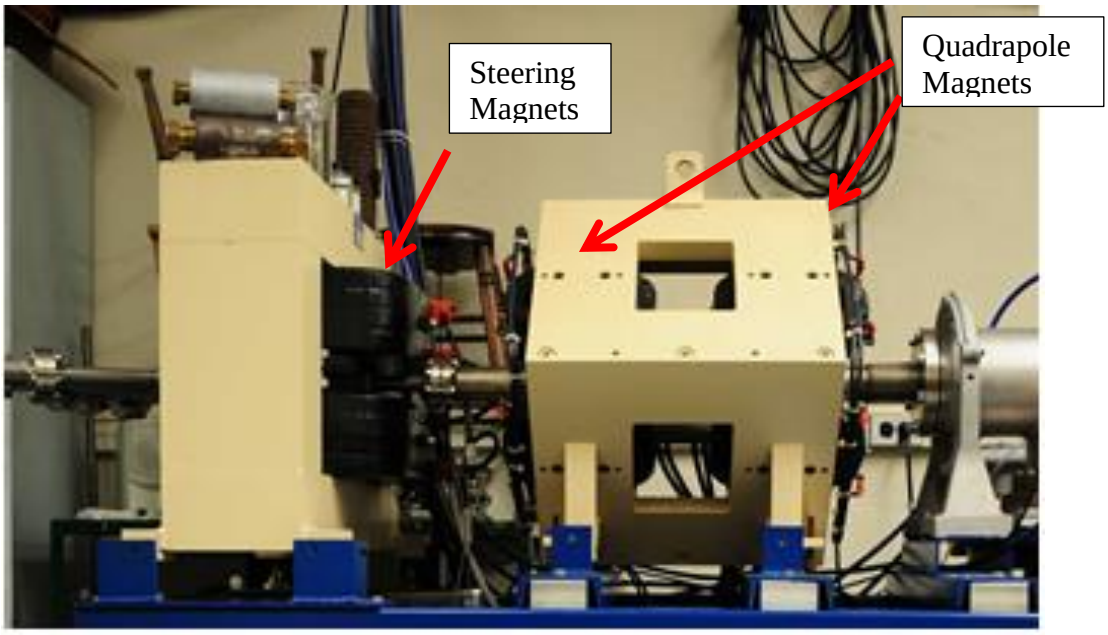

Figure 9: Picture of the quadrapole magnets used to shape the beam and the steering magnets which are used to turn the beam towards the target. In this picture the magnetic field is pointing down the page, the beam is moving right to left and the force on the beam is therefore out of the page by the Lorentz Force Law.

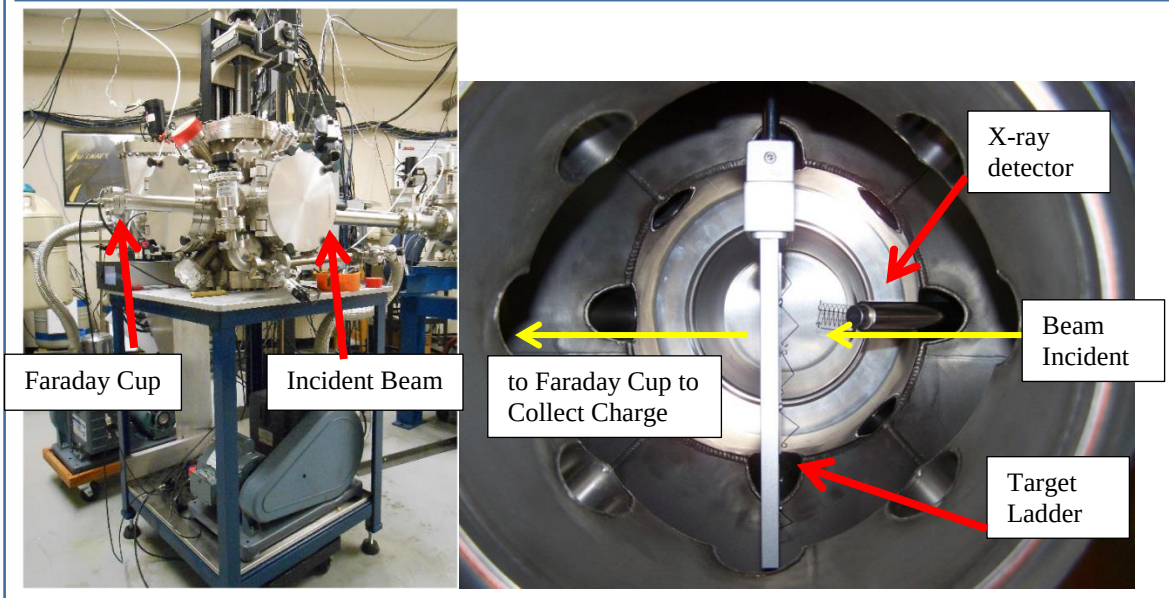

Figure 10: Picture on the left is of the scattering chamber with the incident beam entering from the left and continuing to the Faraday cup on the right. The picture on the right is the inside of scattering chamber showing the target ladder that holds the sample and the nose of the Amptek X-ray detector which is on the right.

2.3 Calibration and Data Analysis

In order to quantitatively analyze data collected from our aerosol samples we needed to calibrate our X-ray spectrum and determine the H-value needed in equation 5 by using standards. We used a program called Amptek ADMCA to display the detected X-rays from the standards being hit by the beam of protons. The program would stop collecting data once we had collected 1μC worth of charge from the beam on target and we did this for 7 standards: Al, Au, Cu, Fe, Ge, Pb, and Ti to span the elements we think are in our aerosol samples. Graphs of intensity of x-rays versus channel number were plotted. A representative sample of Aluminum is shown in Figure 11. To convert the channel number into energy (in keV) we recorded the channel number corresponding to the peak for each standard and used a table[9] to find the energy of each peak based on equation 4. We then plotted the energy (in keV) versus the channel number for the peaks of each standard as shown in Figure 12. Many of the spectra have several peaks which correspond to the different transitions of that element and also any backing that was used to make the standard, like Ca. We find that the relationship is linear and therefore can use the equation from the line of best fit in order to get a conversion from channel number to energy in keV as shown in the equation 10 below. We find

$$Energy = 0.0273 \cdot (channel\ \#) - 0.1299 \qquad [10]$$

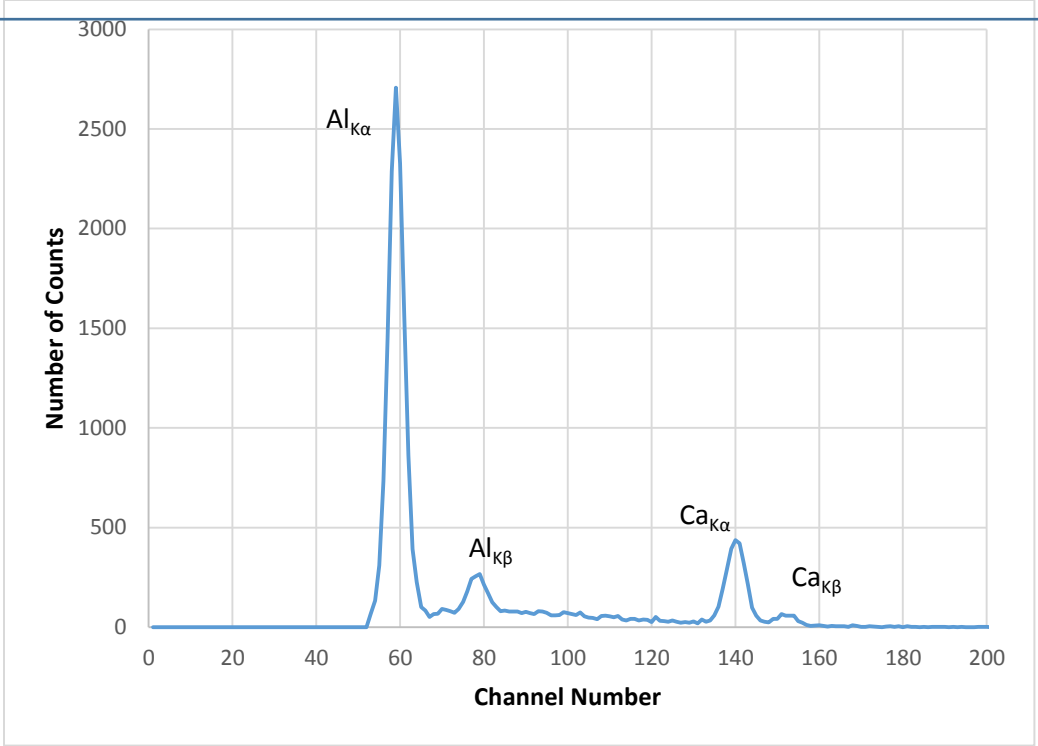

Figure 11: Spectrum for representative sample of the x-ray Al standard showing the number of counts or x-ray intensity versus the channel number. The peaks for the Al are labeled with their corresponding x-ray type and the peaks to the right of the Al peaks are due to Ca from the backing of the standard.

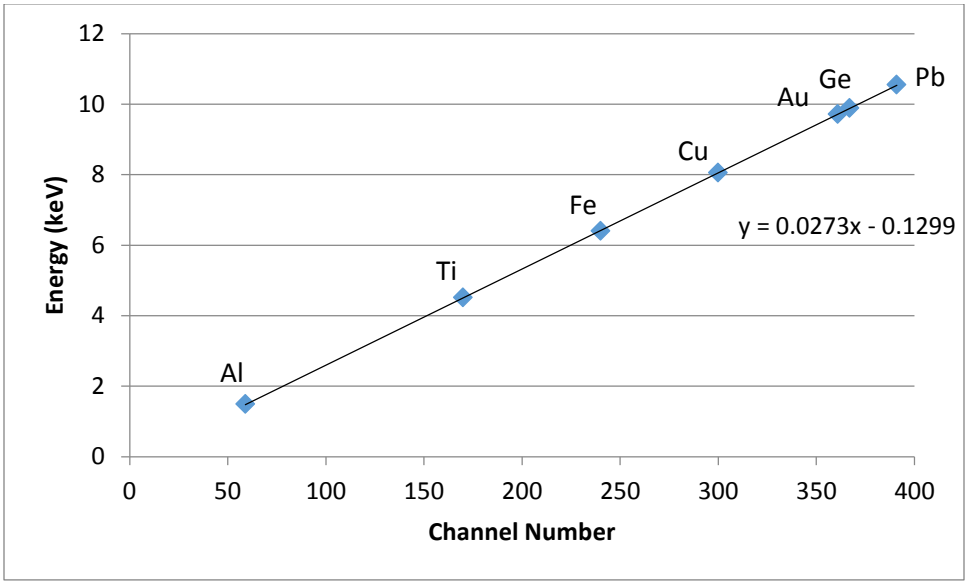

Figure 12: Plot of the energy (in keV) versus the channel number as determined from the peak of each x-ray standard and table of each peaks energy. The fit is used to convert the channel number into energy (in keV).

Having collected our x-ray spectra, the data is transferred to GUPIX. GUPIX is a PIXE analysis tool that determines the concentration of the elements detected using the calibration data from figure 12 based on equation 5. In order for GUPIX to calculate the concentrations using equation 5, the H-value, which is an experimental parameter equal to the solid angle of the detector is needed. Rather than measuring the solid angle of the detector we used the H-value to calibrate our system by initially setting the H-value to 1 and determining the initial concentration of our standards. Then we can determine the corrected H-value by dividing our initial concentrations by the actual concentrations recorded on the standards, as shown in Table 1. If we graph the elements' atomic number versus the corrected H-value we see that the relationship is linear as shown in Figure 13. Finally we averaged all of our new H-values to get a final H-value of 0.000743. After calibrating all our programs, data was collected on our aerosol samples. Each sample collected x-rays until we collected 30μC of charge; we collected more charge than the standards since the amount of Pb will be very small and so we need to collect more x-rays in order to properly detect it. We then used GUPIX to determine concentrations of a range of elements from Al-Pb. We also ran a blank Kapton foil so that we could subtract the background from our samples.

Element (Z)	Actual Concentration (ng/m^2)	Concentration with H=1 (ng/cm^2)	new H value ($C_{H=1}/C_{actual}$)
Al (13)	48100	34.3	0.000713
Au (79)	45600	34.7	0.000761
Cu (29)	60500	44.5	0.000736
Fe (26)	54800	39.8	0.000726
Ge (32)	49000	36.5	0.000745
Pb (82)	52800	42.3	0.000801
Ti (22)	55800	40	0.000717
		Average H-value	0.000743

Table 1: The actual concentrations of standards, concentrations from GUPIX with an inital H-value of 1 and our calculated H-value

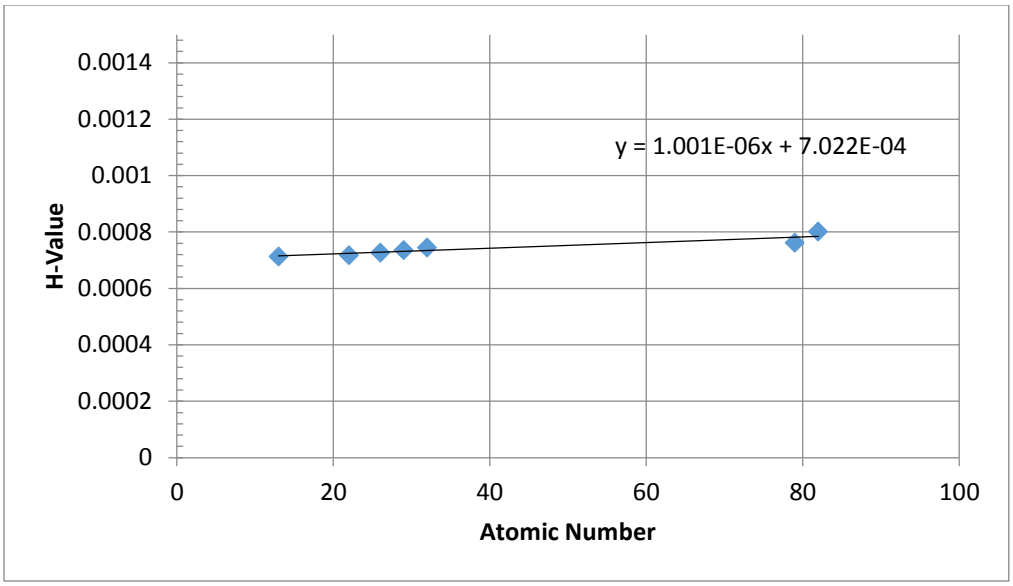

Figure 13: Calculated H-value from each standard versus the atomic number of each standard. The fit tells us that the H-value is nearly constant so we can approximate the actual H-value by simply taking the average of our calculated H-values.

3 Results and Anlaysis

After collecting our data we plotted the energy or intensity spectra, which have x-ray counts versus energy, of each stage along with the blank Kapton foil and use our table of peak energies in order to see which elements were present in each sample as shown in Figure 14. After examining the spectra for which elements were present we used GUPIX to determine the concentrations of these elements in ng/cm^2. From equation 6, along with values from after collection shown in Table 2, we calculated the concentration in terms of ng/m^3, as shown in Figure 15. The sets of data are labeled so the first term represents the sampling site, the second number is the month it was taken and the last number is the year it was taken. All of our data sets showed concentrations of Br and Pb in stage 1 (0.25µm particle size) and stage 2 (0.5µm particle size) which corresponds to particle sizes that can be inhaled into the lungs and cause damage[10]. The fact that we see both Br and Pb in these stages is evidence that the Pb is most likely from aviation fuel emissions, because it contains lead(ll) bromide, an additive to aviation fuel. If this had been an emission from industry or some other source we would only see Pb and no Br. To look at all our samples taken we plotted together the Pb and Br concentrations for stages 1 and 2

as shown in Figure 16 and 17 respectively. We first noticed that the set S1_06_09 contained no Br on either stage and had a lot more Pb in stage 1 than any other of the sets. We do not know why this is, it could have been related to the fact that this set was taken 4 years previous to the other sets. Until we discover the cause of this difference we chose to exclude this set from further data analysis. We also noticed in stage 1, sample sets S1_12_13 and S1_01_14 showed higher Br concentration than Pb concentration and that in stage 2 these were the only sets that had both Br and Pb. We believe the reason that these two sets had most of their Br and Pb in the second stage has perhaps to do with the temperature and the change of season. The drop in temperature and increase in pressure could have caused the particles to be deposited on a different stage or maybe the particles themselves formed differently under colder conditions. Next we made a table comparing the Br/Pb ratios from stage 1 for sets 06-10 and stage 2 for sets 12 and 01 since they were the samples with the largest amounts of Br and Pb. We then averaged these ratios to get an average Br/Pb ratio of 0.443±0.029 as shown in Table 3.

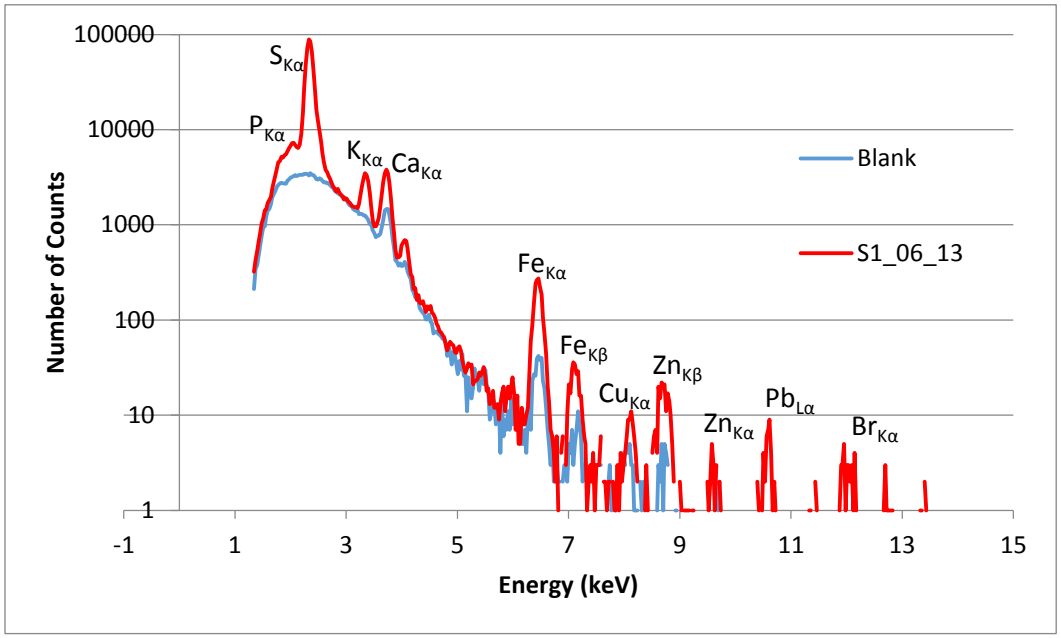

Figure 14: X-ray intensity versus energy spectrum for stage 1 (0.25µm particle size) of a sample collected at the Union College boat house in June 2013 showing number of counts versus energy in keV. The blue line represents the spectrum from blank Kapton and the red is the actual aerosol data on the Kapton backing. The elemental peaks are labeled by x-ray type and notice the only L series transition is from the Pb.

	S1_06_09	S1_06_13	S2_07_13	S1_08_13	S1_10_13	S1_12_13	S1_01_14
t(min)	2656	2875	2880	2850	2880	2781	2944
flow(m^3/min)	0.001	0.001	0.001	0.001	0.0008	0.001	0.001
flow uncert	0.00005	0.00005	0.00005	0.00005	0.0002	0.00005	0.00005
P_{std}(mmHg)	760	760	760	760	760	760	760
T_{std}(K)	298	298	298	298	298	298	298
P (mmHg)	754.634	758.698	763.778	760.73	762.762	766.318	766.572
P uncert	2.54	2.54	5.08	3.81	3.81	1.27	2.54
T (K)	293	298.6	296.3	294.1	288	266.89	264.67
T uncert	1.7	1.15	0.55	0.55	1.7	2.22	6.11

Table 2: Measured values of time, flow, temperature, and pressure during which the samples were being collected. These values are used in equation 6 in order to calculate the concentrations in terms of ng/m^3 as shown in the next figure

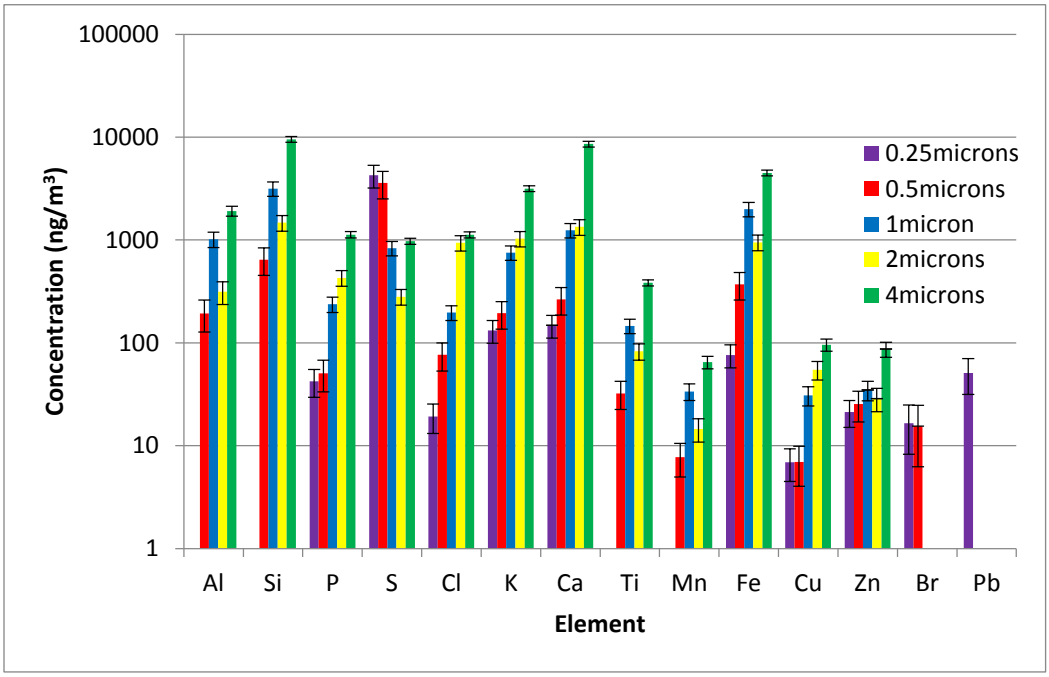

Figure 15: Concentrations for the first five stages (sizes 0.25µm - 4µm) of a sample collected at the Union College boat house in June 2013 showing the concentration in ng/m^3 versus Z where each color represents a different size particle.

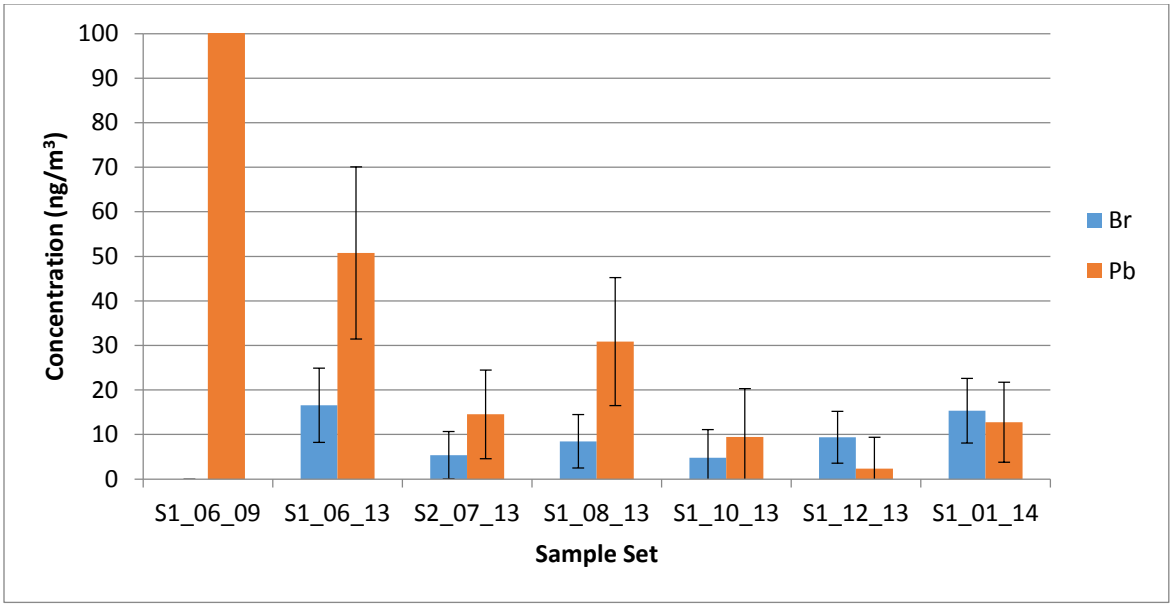

Figure 16: Concentrations of Br (blue) and Pb (orange) from the first stage (0.25µm) of each sample set.

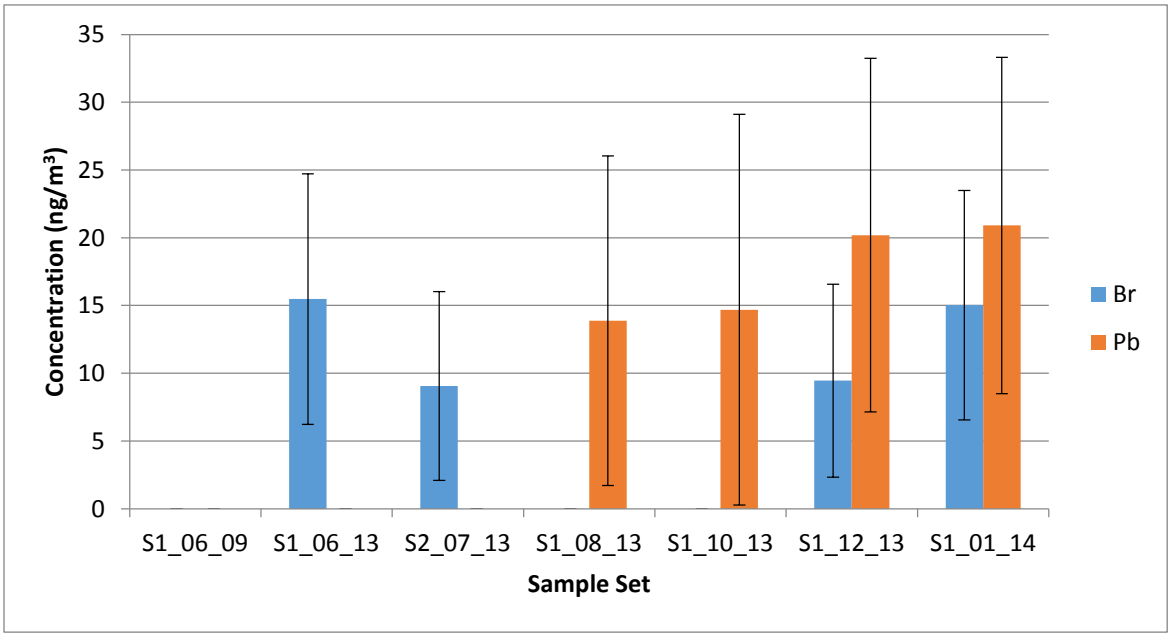

Figure 17: Concentrations of Br (blue) and Pb (orange) from the second stage (0.5µm) of each sample set.

Sample Set	Br conc (ng/m^3)	Pb conc (ng/m^3)	Br/Pb ratio
BH06_13	16.56±8.33	50.73±19.32	0.326±0.039
JB07_13	5.33±5.32	14.52±9.93	0.367±0.116
BH08_13	8.47±5.99	30.87±14.36	0.274±0.066
BH10_13	4.76±6.30	9.47±10.83	0.503±0.090
BH12	9.46±7.12	20.19±13.04	0.468±0.050
BH01	15.02±8.47	20.91±12.41	0.719±0.021
		Average ratio	0.443±0.029

Table 3: Concentrations of Br, Pb, and ratio of Br/Pb for all sample sets, where S1 and S2 are the first and second sampling site respectively and the following numbers are the month and year they were taken. Sets 06-10 are from stage 1 and sets 12 and 01 are from stage 2.

Conclusions

Our goals for this experiment were to examine aerosol samples collected near the Schenectady County Airport to see if we could find any Pb, if Pb is detected can we identify it as being tetraethyl lead used by aviation gas and whether or not the Pb concentrations vary by season or by location with respect to the airport. In all our sets of samples we consistently found Pb in stages 1 and 2 which corresponds to particles on the scale of 0.25-0.5μm. These size particles can be inhaled into the lungs and therefore if there was enough of a substance, it could cause one harm[10]. However, the most amount of lead we are seeing is on the order of $100ng/m^3$ which is insignificant when compared to the most common elements present in the aerosol samples, such as Si and Ca which are on the order of $10000ng/m^3$. We also notice that the Pb in the set taken at sampling site 2 is considerably lower than that of the sets taken at sampling site 1 around the same time. We believe this is due to the fact that sampling site 2 is perpendicular to the main runway so there is less air traffic in that area compared to sampling site 1 which is directly in the takeoff path of the main runway. We can therefore conclude that the location with respect to the main runway and take off patterns will affect the amount of emissions detected.

We also consistently see Br in stages 1 and 2 of our sets of data which is characteristic of aviation fuel emissions due to the use of lead(ll) bromide. Therefore we can correctly identify this Pb in the air as aviation emission since if it had been from

industry or some other source we would not see the Br. However, we only see Pb in our first set of samples taken in 2009. We also notice that this set has a much larger amount of Pb compared to the other sets. We have concluded that this set of data is an outlier perhaps due to the fact that it was taken 4 years before the other sets of samples. We also noticed in stage 1 that sample sets S1_12_13 and S1_01_14 had more Br than Pb and that in stage 2 these were the only sets that had both Br and Pb. We believe the reason that these two sets had most of their Br and Pb in the second stage has to do with the temperature and the change of season. Since the impactor works by depositing the different size particles using the flow of air and pressure, the drop in temperature and increase in pressure could have caused the particles to be deposited on a different stage. Another possibility is maybe the particles themselves formed differently under colder conditions, since the colder it is the denser the atmosphere will be causing different formations of particles. This is all speculation and we need to research this area further and gather more data.

Finally we compared the amount of Br to Pb using a ratio and took the average, excluding our first set of data, in order to compare our value to known values of Br/Pb for leaded gas emissions. We got an average value of 0.443±0.029 for our Br/Pb ratio and the measured value from O'Connor et al in Perth Australia during the 1970's was 0.59±0.05 while the measured value in the US was 0.25±0.03[1]. While our results do not match that from Perth Australia it is also not consistent with the measured values in the US. If we take into account that in Perth they had a lot more leaded gas emission due to the use of leaded gas by automobiles at the time, the ratio may be different from ours since only small aircraft are using leaded fuel in our area. On the other hand, the US ratio is for an area with leaded fuel only being used by small aircrafts, so why doesn't our value match this. It could possibly be because our samples were taken in such close proximity to the main runway whereas we do not know the exact locations of the previous studies made in the US. We also noted that O'Connor et al noticed that the Br/Pb ratio during the mid-winter was larger than the ratio during the mid-summer[2]. We do notice an increase from June through January for our data, excluding the set taken in August. We believe the set of data from August does not follow this trend, because while collecting particles the impactor's flow rate dropped off, which could affect our concentration results.

We initially wanted to answer 4 questions: can we detect any Pb in the air samples by particle induced x-ray emission spectroscopy, if Pb is detected, can we identify it as being from tetraethyl lead used in aviation gas, and whether or not the Pb concentrations vary by season or by the location with respect to the airport. We were definitely able to detect Pb in all of our air samples in the area with concentrations on the order of $30ng/m^3$. We also detected Br in the samples and a ratio of 0.443 ± 0.029 for Br/Pb. Based on previous studies in the 70s this is somewhat consistent with emission from aviation fuel; however no recent studies have been made on this subject. We also observed that the ratio of Br/Pb was larger during the mid-winter than in the mid-summer which agrees with previous studies. Finally, we found that if the location of the sampling site was directly in line with the main runway, more Pb was observed than from a sampling site that was perpendicular from the main runway. Overall we find our data to be consistent with previous studies and we believe that the Pb that we find in the air to be originating from the local airport's aviation emission. We plan on taking more data in order to get a better idea of the seasonal variations and to get a more accurate value for our Br/Pb ratio.

References

[1] B. H. O'Connor, G. C. Kerrigan, W. W. Thomas, A.T. Pearce. *Use of Bromine Levels In Airborne Particulate Samples to Infer Vehicular Lead Concentration in the Atmosphere*. Atmospheric Environment Vol. 11, pp. 635-638. Dec 1976

[2] B. H. O'Connor, G. C. Kerrigan, C.R. Nouwland. *Temporal Variation in Atmospheric Particulate Lead and Bromine Levels for Perth Western Australia (1971-1976).* Atmospheric Vol. 12, pp. 1907-1916. Feb 1978.

[3] Diagram Modified from http://fys.kuleuven.be/iks/nvsf/experimental-facilities/particle-induced-x-ray-emission-pixe

[4] Diagram Modified from http://ie.lbl.gov/xray/xrf.htm

[5] S. Johansson, J. Campbell, K. Mamguist, J. Wiley. *Particle Induced X-ray Emission Spectroscopy (PIXE).* Sons Inc, 1995.

[6] https://www.google.com/maps/@42.8544221,-73.928535,5013m/data=!3m1!1e3

[7] PIXE International Corporation. http://www.pixeintl.com/Impactor.asp

[8] National Electrostatic Corporation. http://www.pelletron.com/tutor.htm

[9] http://minerva.union.edu/labrakes/xrayenergytable.pdf

[10] Hinds, William C. (1999). Aerosol Technology (2nd ed.). Wiley - Interscience.

[11] https://www.airnav.com/airport/KSCH

Appendix

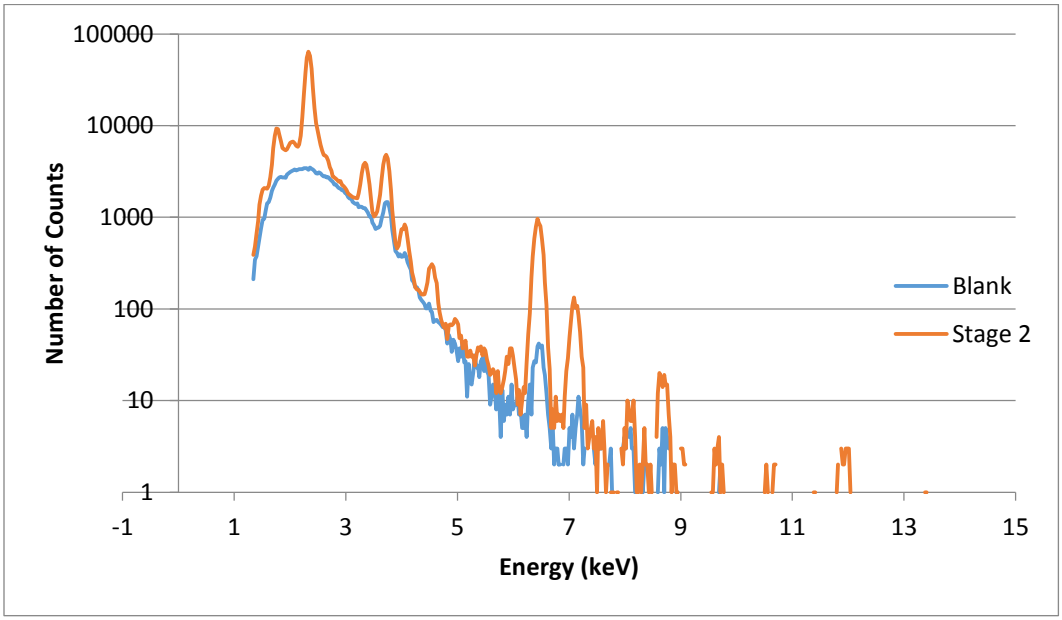

Figure A1: X-ray intensity versus energy spectrum for stage 2 (0.5µm particle size) of a sample collected at the Union College boat house in June 2013 showing number of counts versus energy in keV. The blue line represents the spectrum from blank Kapton and the red is the actual aerosol data on the Kapton backing.

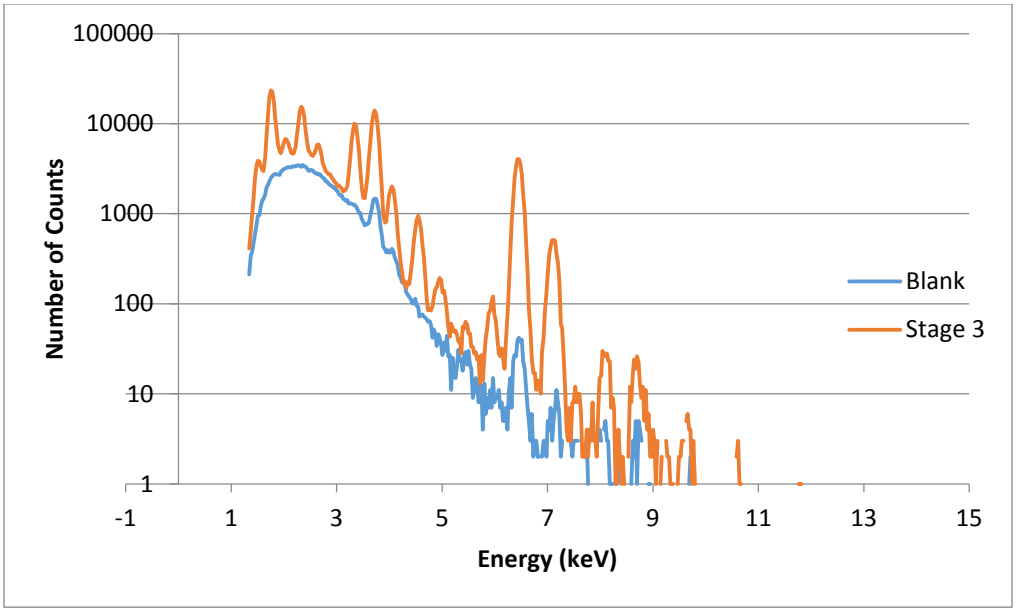

Figure A2: X-ray intensity versus energy spectrum for stage 3 (1µm particle size) of a sample collected at the Union College boat house in June 2013 showing number of counts versus energy in keV. The blue line represents the spectrum from blank Kapton and the red is the actual aerosol data on the Kapton backing.

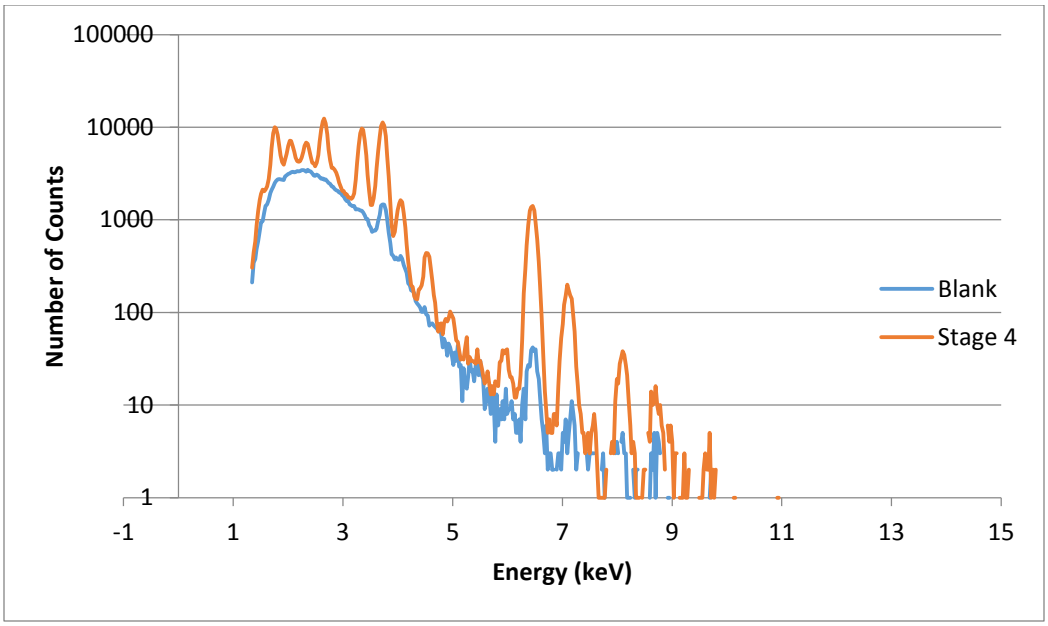

Figure A3: X-ray intensity versus energy spectrum for stage 4 (2µm particle size) of a sample collected at the Union College boat house in June 2013 showing number of counts versus energy in keV. The blue line represents the spectrum from blank Kapton and the red is the actual aerosol data on the Kapton backing.

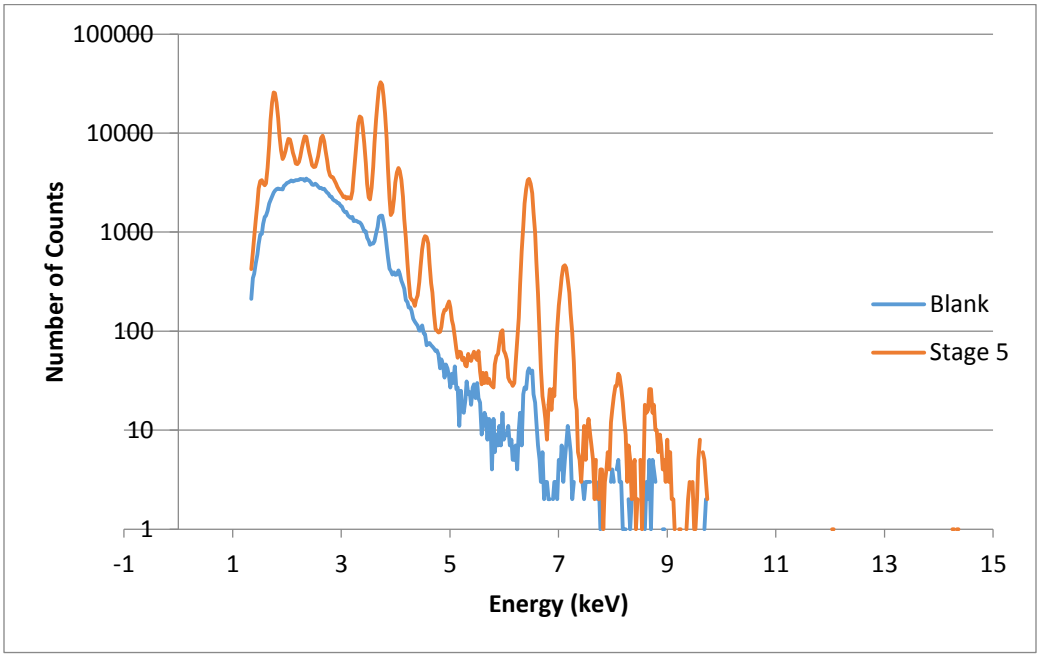

Figure A4: X-ray intensity versus energy spectrum for stage 5 (4µm particle size) of a sample collected at the Union College boat house in June 2013 showing number of counts versus energy in keV. The blue line represents the spectrum from blank Kapton and the red is the actual aerosol data on the Kapton backing.

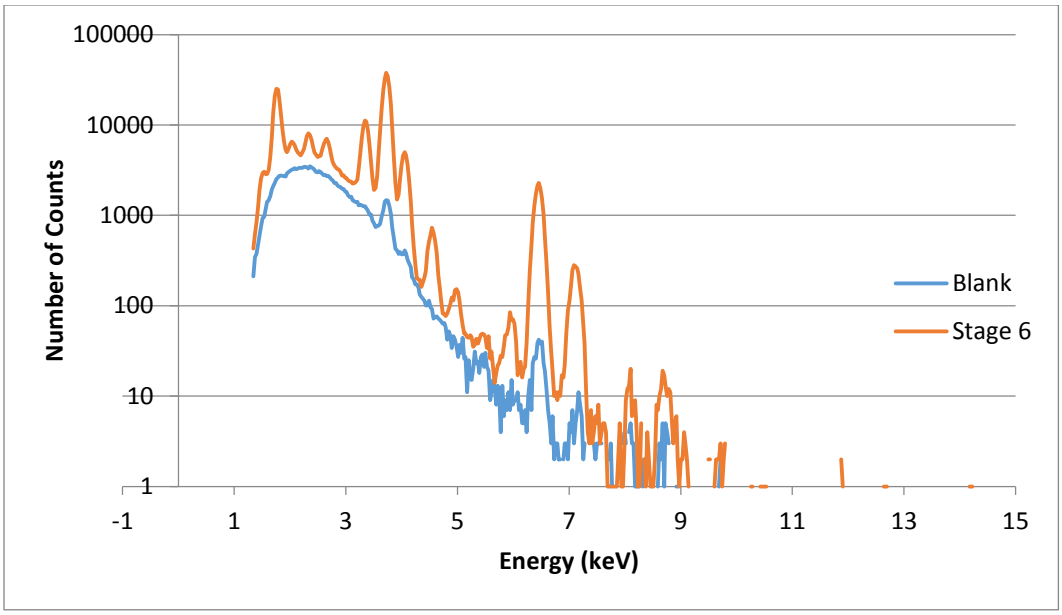

Figure A5: X-ray intensity versus energy spectrum for stage 6 (8µm particle size) of a sample collected at the Union College boat house in June 2013 showing number of counts versus energy in keV. The blue line represents the spectrum from blank Kapton and the red is the actual aerosol data on the Kapton backing.

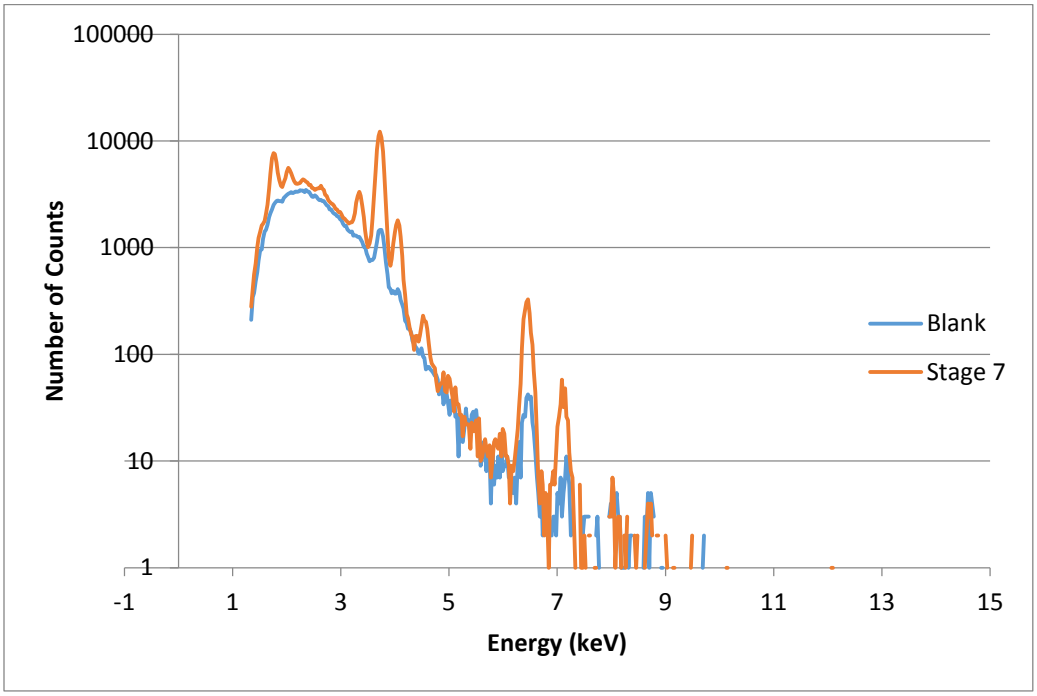

Figure A6: X-ray intensity versus energy spectrum for stage 7 (16µm particle size) of a sample collected at the Union College boat house in June 2013 showing number of counts versus energy in keV. The blue line represents the spectrum from blank Kapton and the red is the actual aerosol data on the Kapton backing.

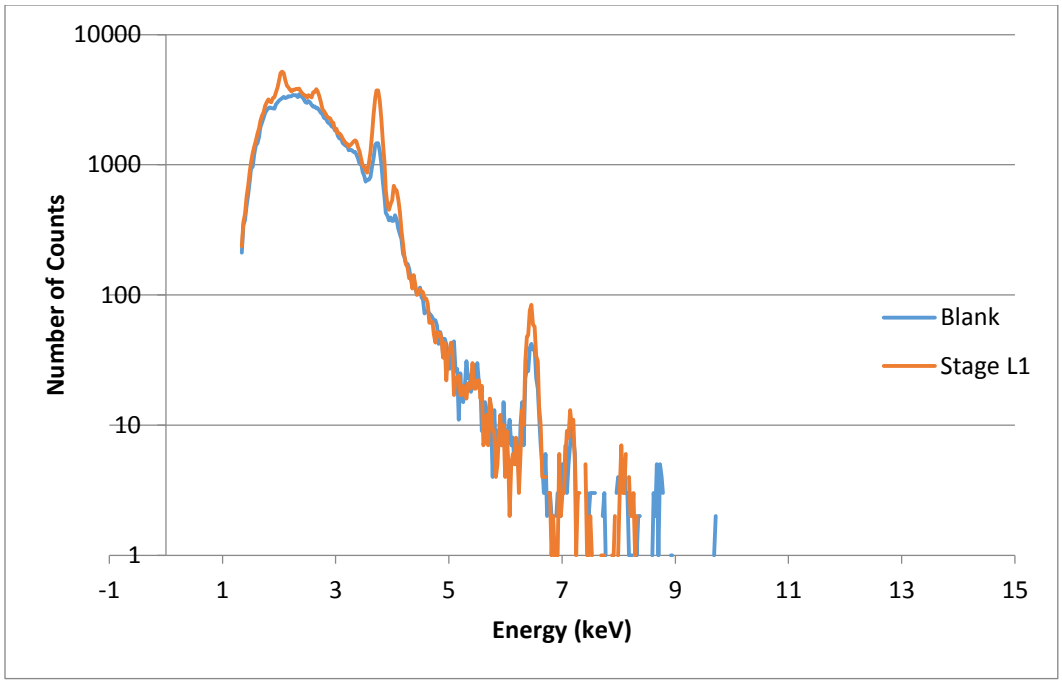

Figure A7: X-ray intensity versus energy spectrum for stage L1 (0.06µm particle size) of a sample collected at the Union College boat house in June 2013 showing number of counts versus energy in keV. The blue line represents the spectrum from blank Kapton and the red is the actual aerosol data on the Kapton backing.

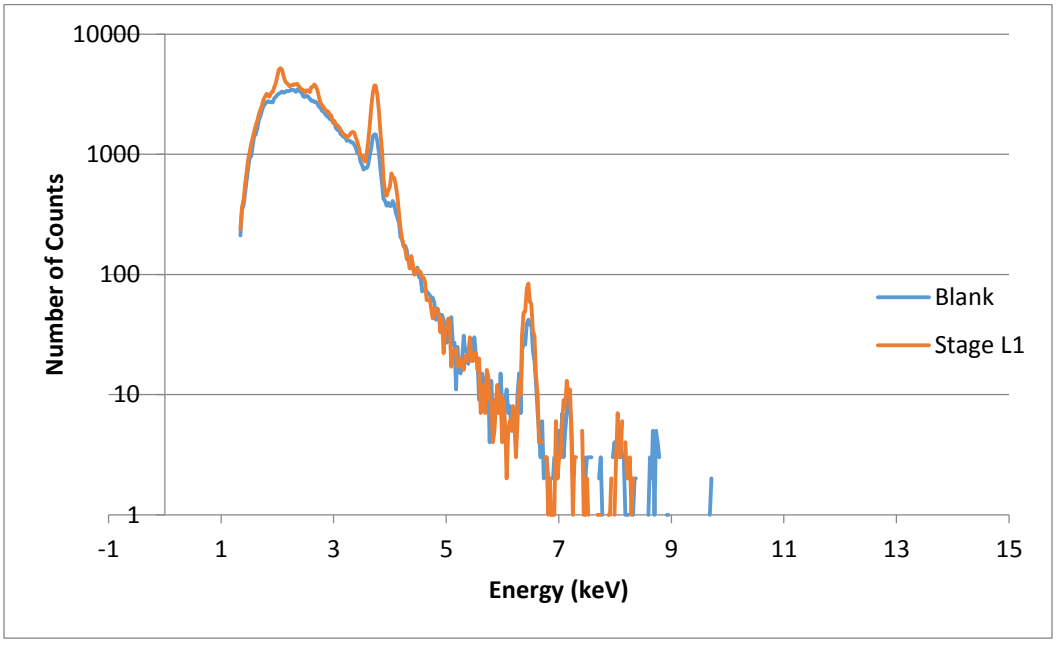

Figure A8: X-ray intensity versus energy spectrum for stage L2 (0.12µm particle size) of a sample collected at the Union College boat house in June 2013 showing number of counts versus energy in keV. The blue line represents the spectrum from blank Kapton and the red is the actual aerosol data on the Kapton backing.

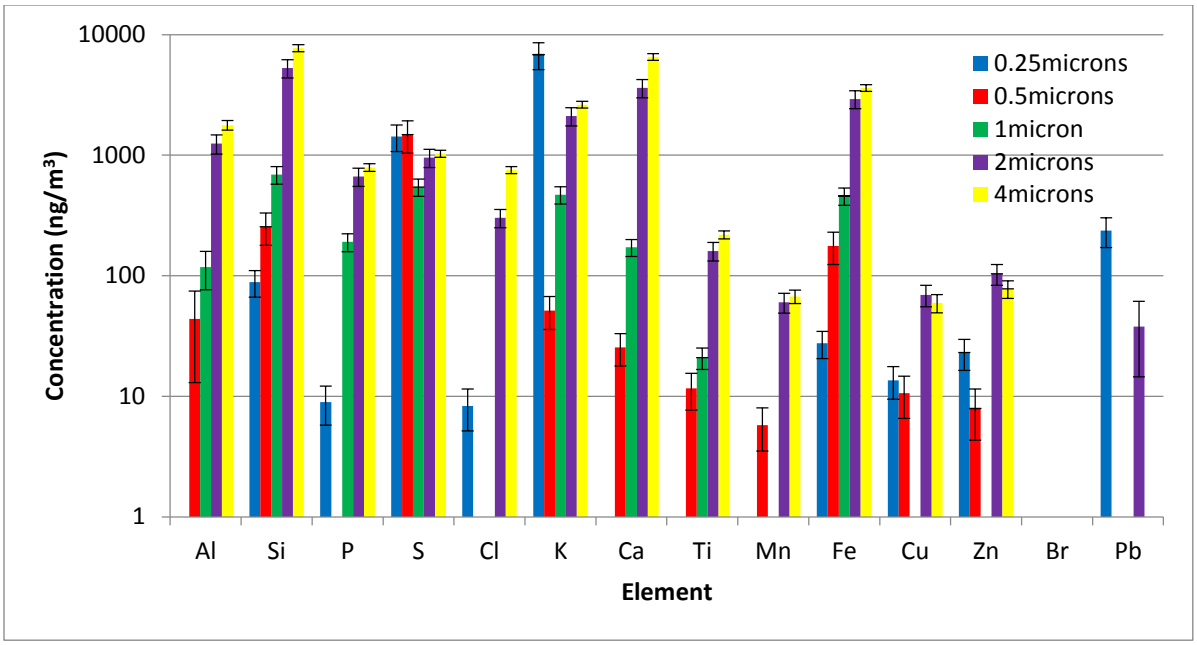

Figure A9: Concentrations for the first five stages (sizes 0.25µm - 4µm) of a sample collected at the Union College boat house in June 2009 showing the concentration in ng/m^3 versus Z where each color represents a different size particle.

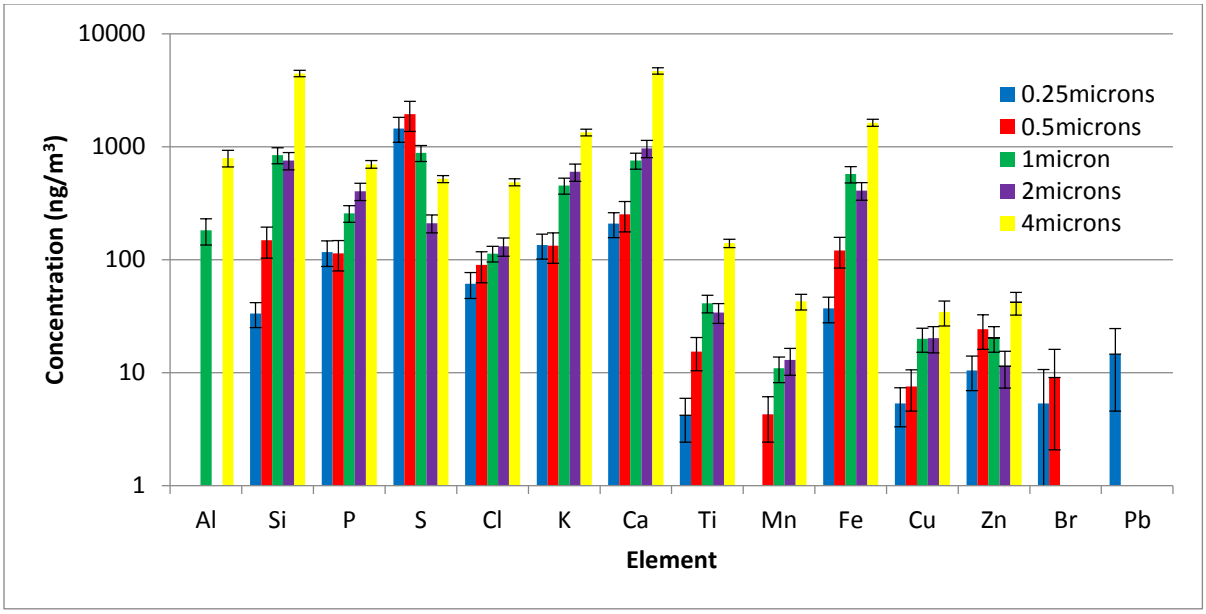

Figure A10: Concentrations for the first five stages (sizes 0.25µm - 4µm) of a sample collected at Sampling Site 2 in July 2013 showing the concentration in ng/m^3 versus Z where each color represents a different size particle.

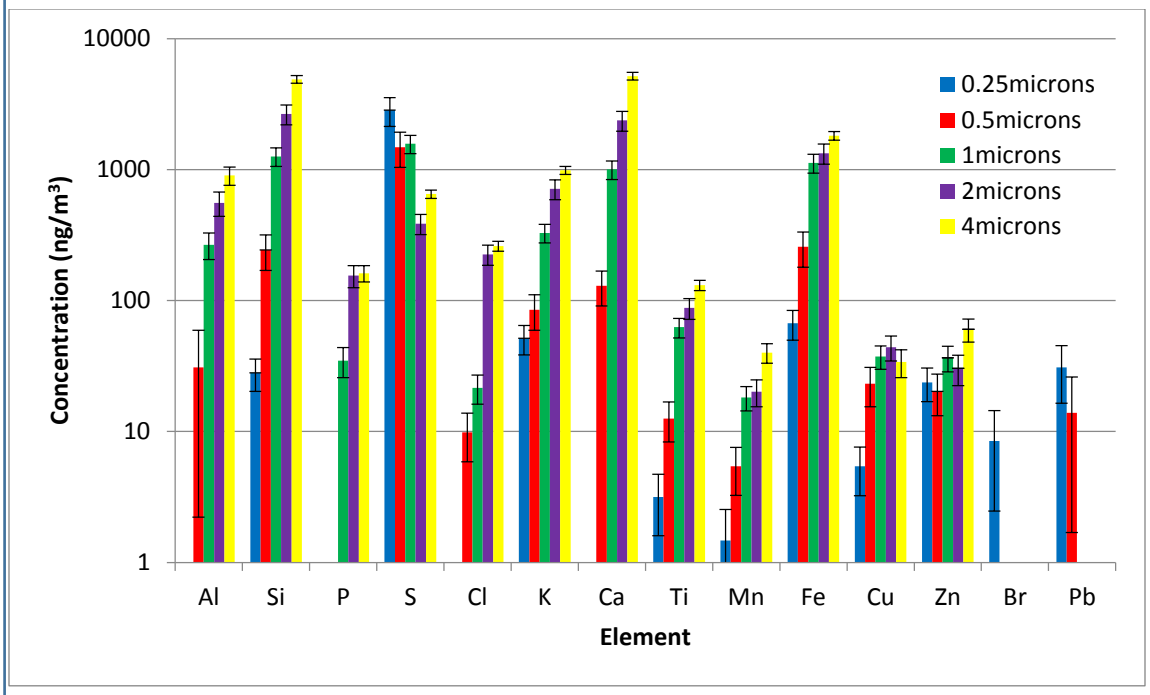

Figure A11: Concentrations for the first five stages (sizes 0.25µm - 4µm) of a sample collected at the Union College boat house in August 2013 showing the concentration in ng/m^3 versus Z where each color represents a different size particle.

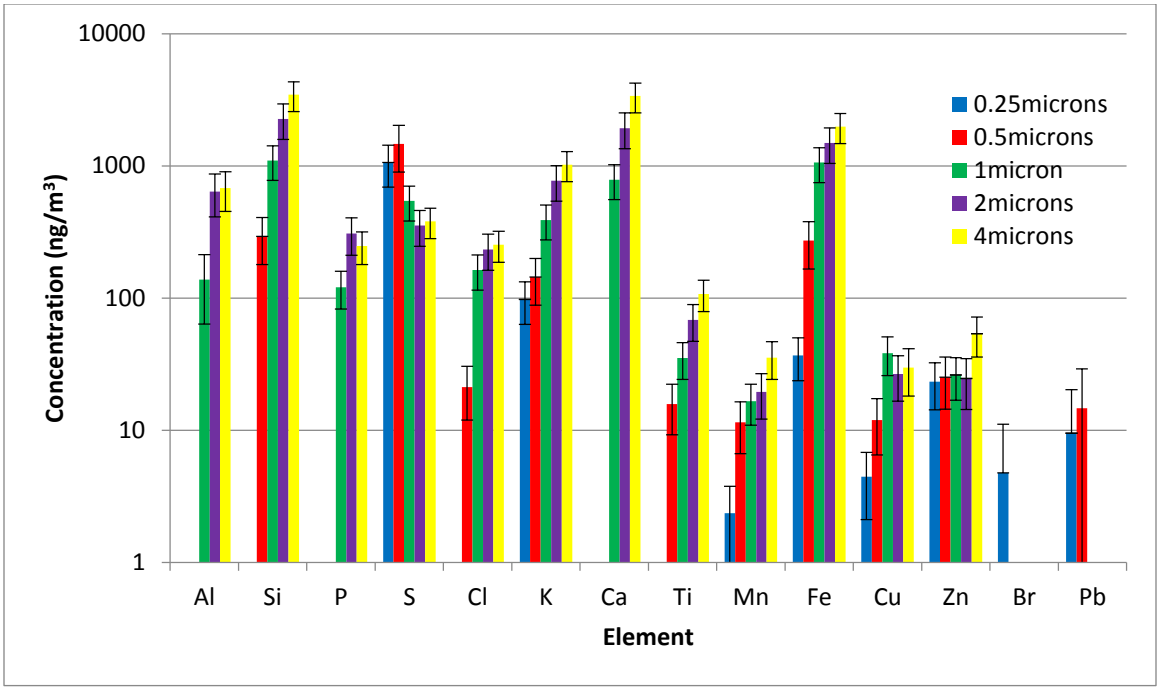

Figure A12: Concentrations for the first five stages (sizes 0.25µm - 4µm) of a sample collected at the Union College boat house in October 2013 showing the concentration in ng/m^3 versus Z where each color represents a different size particle.

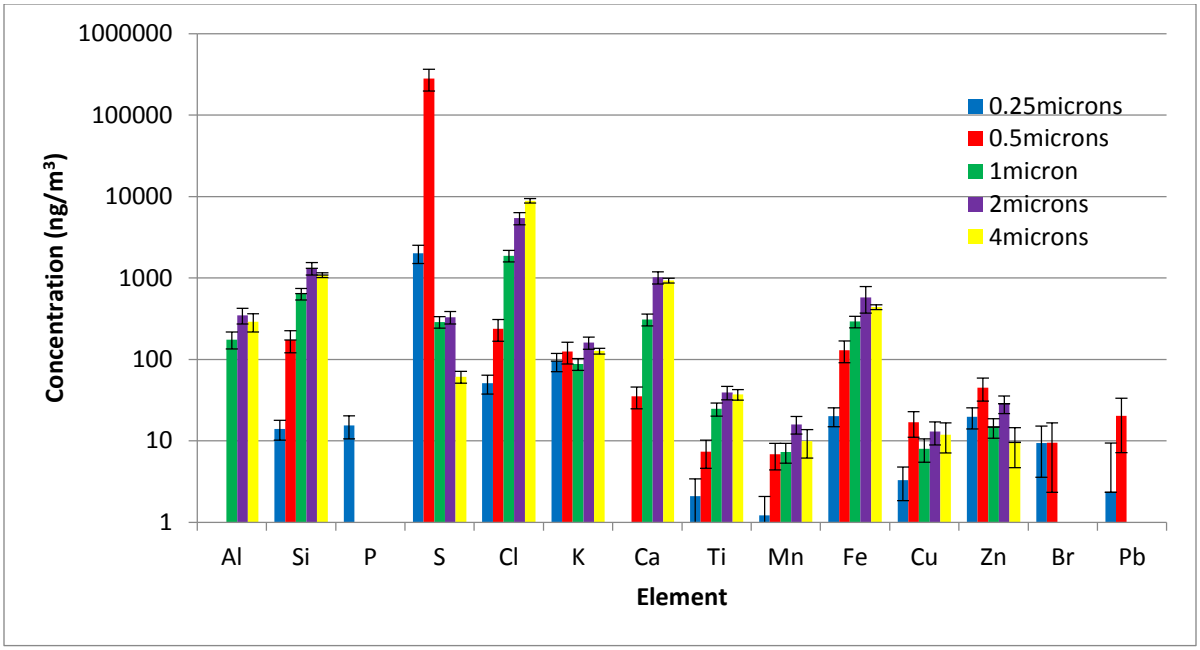

Figure A13: Concentrations for the first five stages (sizes 0.25µm - 4µm) of a sample collected at the Union College boat house in December 2013 showing the concentration in ng/m^3 versus Z where each color represents a different size particle.

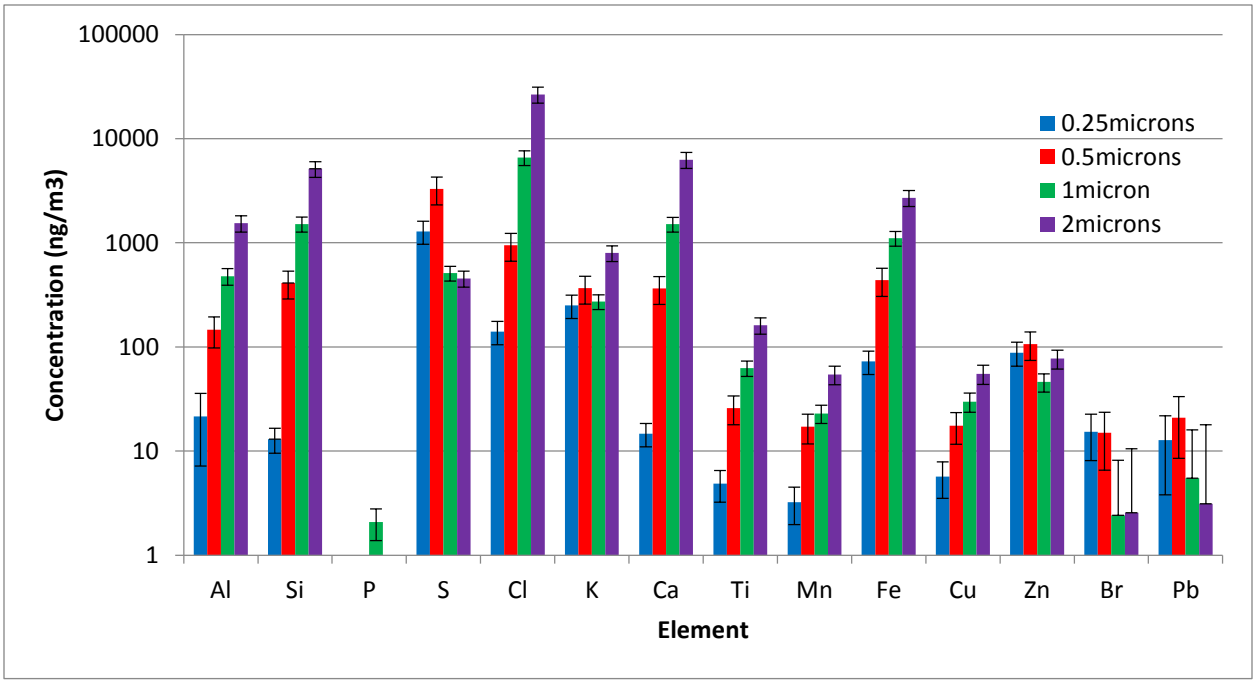

Figure A14: Concentrations for the first five stages (sizes 0.25µm - 4µm) of a sample collected at the Union College boat house in January 2014 showing the concentration in ng/m^3 versus Z where each color represents a different size particle.